Sensors and Materials, Vol. 20, No. 5 (2008) 211–219
MYU Tokyo

S & M 0719

Gas Sensing Characteristics of Nanocrystalline $Ba_{0.5}Sr_{0.5}MoO_4$ Thick Film Prepared by Sol-Gel Method

Mohammad Reza Vaezi

Advanced Materials Research Center, Materials and Energy Research Center, Karaj, Iran

(Received December 24, 2007; accepted July 18, 2008)

Key words: thick-film gas sensor, $Ba_{0.5}Sr_{0.5}MoO_4$, sensitivity, doping

Thick-film gas sensors were fabricated from nanocrystalline pure and doped $Ba_{0.5}Sr_{0.5}MoO_4$ powders; fine and homogeneously sized powders were prepared using chemical methods such as sol-gel technique. X-ray diffraction (XRD) has confirmed the formation of nanocrystalline $Ba_{0.5}Sr_{0.5}MoO_4$ structure (JCPDS 30–157) for sol-gel powders after annealing. The results obtained from XRD and transmission electron microscope (TEM) show that the powders have nanocrystalline structure and the mean particle sizes of $Ba_{0.5}Sr_{0.5}MoO_4$ powders with and without CuO are approximately 33 and 21.8 nm, respectively. The gas sensing measurements indicate that the $Ba_{0.5}Sr_{0.5}MoO_4$ sensors show good response to H_2S and poor response to other reducing gases such as H_2, LPG, and CO. The sensitivity was improved by the incorporation of CuO as an additive in $Ba_{0.5}Sr_{0.5}MoO_4$. The maximum sensitivity was obtained for $Ba_{0.5}Sr_{0.5}MoO_4$ with 4 wt% CuO at an operating temperature of 250°C. Also, Pd doping over $Ba_{0.5}Sr_{0.5}MoO_4$ with 4 wt% CuO decreases the operating temperature from 250 to 200°C while increasing the sensitivity to H_2S.

1. Introduction

The recent concern over environmental pollution and increased awareness of the need to monitor hazardous gases has stimulated substantial interest in sensors for the gases CO, CO_2, NO_x, and H_2S. The need to detect and monitor these gases has led to the development of a wide variety of solid-state gas sensors.[1–5] Although several attempts have been made to modify conventional materials, nanostructured gas sensing materials are considered to be advantageous owing to their simplicity of miniaturization. Also, nanocrystalline materials, exhibiting small particle size and large surface area, may be applied to gas sensors for which an excellent surface effect is required. In recent years, nanosized materials associated with a high surface activity, owing to their small particle size and enormous surface area, have been widely used as gas sensors.[6–8]

*Corresponding author: e-mail: vaezi9016@yahoo.com

H_2S monitoring is increasing in importance in industrial areas where H_2S is usually present as an air pollutant. H_2S is disagreeable because of its smell and is also dangerous when present at high concentrations; a small amount of H_2S can also have considerable effects on some industrial processes that utilize sensitive catalysts. Chemical sensors have an enormous potential in the development of instruments that detect dangerous and contaminating gases. Sensors producing electrical signals simulated by low concentrations of gas are currently marketed, but their poor reproducibility and selectivity make them inadequate for the reliable detection of very low concentrations of a pollutant.[9] The detection of the volatile sulfide H_2S with SnO_2-based sensors has so far been attempted.[10] The addition of small amounts of additives is known to improve the sensitivity.[11–15]

There has been much interest in perovskite-structured compounds because of their unique catalytic action[16] and gas sensing properties.[17–21] The materials are highly defective and have oxygen- deficient structures, in which the valence state of metal ions may be controlled by temperature, oxygen partial pressure, and dopants.[22] Moreover, to improve selectivity for a particular application, surface modification by the proper choice of additives or dopants to the base material is often used. The doping is generally based on the selection of the most effective catalysts, which modulate a specific chemical reaction on the semiconductor sensor surface. The noble metals, well known as active catalysts, have been confirmed to possess the promoting effects on many semiconductor gas sensors.[23–25] Manorama *et al*. reported the preparation of $BaSnO_3$ doped with noble metals (Pd, Pt, Ru, and Ag). All these results suggested that noble metals play vital roles in the sensor response improvements, of gas sensors.

In this study, the effect of Pd as a dopant on the sensing characteristics of CuO-incorporated $Ba_{0.5}Sr_{0.5}MoO_4$ thick films for H_2S sensing has been investigated.

2. Experimental Procedure

2.1 *Preparation of $Ba_{0.5}Sr_{0.5}MoO_4$ nanopowders and characterization*

$Ba_{0.5}Sr_{0.5}MoO_4$ powder was obtained by the sol-gel method. A stoichiometric mixture of $Ba(NO_3)_2 \cdot 6H_2O$, $Sr(NO_3)_2$ as nitrates and $(NH_4)_6Mo_7O_{24} \cdot 4H_2O$ was added dropwise to citric acid and ethylene glycol under vigorous stirring conditions. The prepared mixture was stirred at 50°C for 2 h to yield a homogeneous mixture. The solution was further heated in a pressure vessel at approximately 120°C for 8 h and subsequently kept at 350°C for 2 h. The dried powder was then annealed at 600°C to improve its crystallinity. The solution of $Cu(NO_3)_2 \cdot 3H_2O$ was used as an additive in the precursors of $Ba_{0.5}Sr_{0.5}MoO_4$.

Pd as a noble metal was doped on $Ba_{0.5}Sr_{0.5}MoO_4$ with 4 wt% CuO. Therefore, an appropriate quantity of the Pd chloride solution was added to the nitrate mixture.

XRD was used to determine the phase present and structure of the powder. A Philips Xpert-Pro X-ray diffractometer with Cu Kα radiation (λ = 1.5418 Å) was employed to obtain XRD spectra using standard θ-2θ geometry. A computer-based search and matching was used for phase identification. The average crystallite size of the powder was estimated with the Scherrer equation using the diffraction intensity of all prominent

lines. The structural properties of the powders were examined using a transmission electron microscope.

2.2 *Sensor fabrication and measurements*

The annealed powder was mixed with 2% polyvinyl alcohol, PVA, as a binder and 5% ethanol as a solvent. The paste obtained was coated (thick-film fabrication method) onto an alumina tube as the substrate. The metallization was carried out by paste printing of a high-temperature conductive epoxy resin (Duralco-124). Two electrodes of 2×4 mm^2 were deposited on each device. Thin gold wires were cemented to the metallized area by the same epoxy. The sample was then gradually heated to 400°C for epoxy curing and contact stabilization. The metal contacts were determined to be ohmic. The substrate was then attached to a temperature-controlled microheater, and was mounted on a refractory stand, so that the temperature of the substrate could be adjusted in the 25–450°C temperature range. The structure of the device is schematically presented in Fig. 1(a). A sensor probe was formed by mounting the sample on a thick-walled borosilicate glass tubing, through which two insulated connection cables were guided to the temperature control unit and the impedance measurement device, respectively (Fig. 1(b)). For each sensitivity measurement, the sensor probe was set at the desired operating temperature (50–400°C) and the probe temperature was allowed to stabilize for 10 min. A load resistor, R_L, was connected in series to the sensor element, R_S. Then, a constant AC voltage (10 V, 80 HZ) was applied across R_L and R_S. DC fields could cause ionic migration and electrode instability, which were of much lesser concern with the use of AC voltage. Test gases were passed into the borosilicate glass tube. The resistance of the sensor was determined by measuring the voltage drop, V_S, across the sensor element. A chromel-alumel thermocouple (TC) was placed on the device to indicate the operating temperature. The schematic of the measurement setup is shown in Fig. 2. To avoid errors caused by the condensation of the contaminating gas on the walls of the tube, it was externally heated to 50°C.

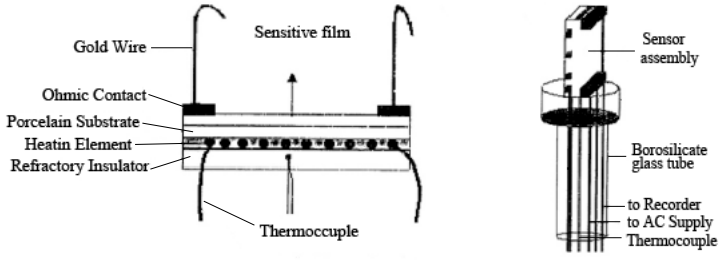

Fig. 1. Schematic illustrations of fabricated gas sensor (a) and sensor probe (b).

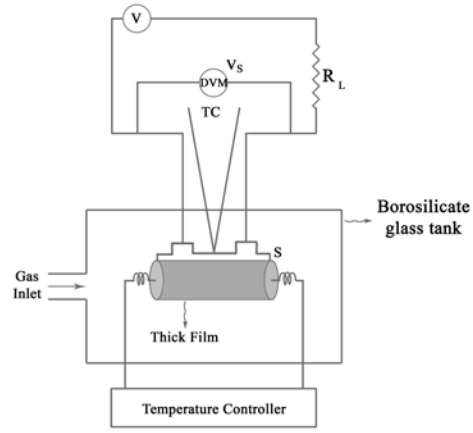

Fig. 2. Schematic of setup used for measuring the change in resistance upon exposure to gases. V, supply voltage; S, sensor probe; DVM, digital voltmeter.

Different definitions of the sensitivity of a gas sensor to a particular target gas, TG, have been presented in the background literature.[26–28] In this paper, the sensitivity of the sensor, *S*, is defined as

$$S = \frac{R_g}{R_a},$$

in which R_g and R_a are the steady-state resistances of the sensor in gas-contaminated air and pure air, respectively. According to this definition, R_g and R_a should both be measured at the operating temperature of the device. To calculate *S*, the electrical resistance of the sensor element was measured in the presence of H_2S at a concentration of 1000 ppm in dry air. The sensitivity of the fabricated sensor to other reducing gases such as H_2, LPG, and CO was also studied.

3. Results and Discussion

The XRD pattern of $Ba_{0.5}Sr_{0.5}MoO_4$ powder annealed at 600°C for 5 h is shown in Fig. 3. From the XRD patterns, we can determine that the crystallite sizes of $Ba_{0.5}Sr_{0.5}MoO_4$ samples with and without CuO are approximately 38 and 25 nm, respectively. These values were calculated from the Scherrer formula applied to the intense peak, (103). Also, it can be seen that the XRD pattern of the $Ba_{0.5}Sr_{0.5}MoO_4$ sample with 4 wt% CuO contains complete phase formation and its crystallinity increases indicating the formation of a solid solution. No extra peaks due to the incorporation of CuO in the $Ba_{0.5}Sr_{0.5}MoO_4$ sample are observed.

TEM images of $Ba_{0.5}Sr_{0.5}MoO_4$ samples with and without CuO are shown in Fig. 4. It is shown that the samples have particulate morphologies with quite uniform grain size distribution. The average grain diameters of the samples with and without CuO are 33

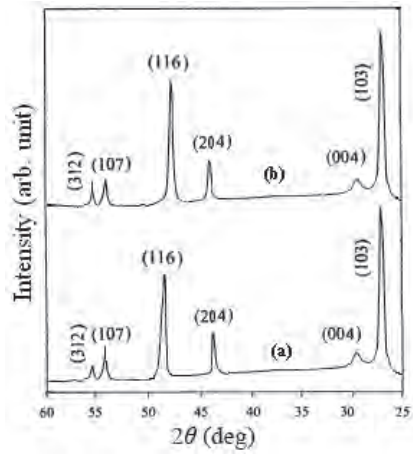

Fig. 3. XRD pattern of $Ba_{0.5}Sr_{0.5}MoO_4$ powder without the incorporation of CuO (a) and with 4 wt% CuO (b).

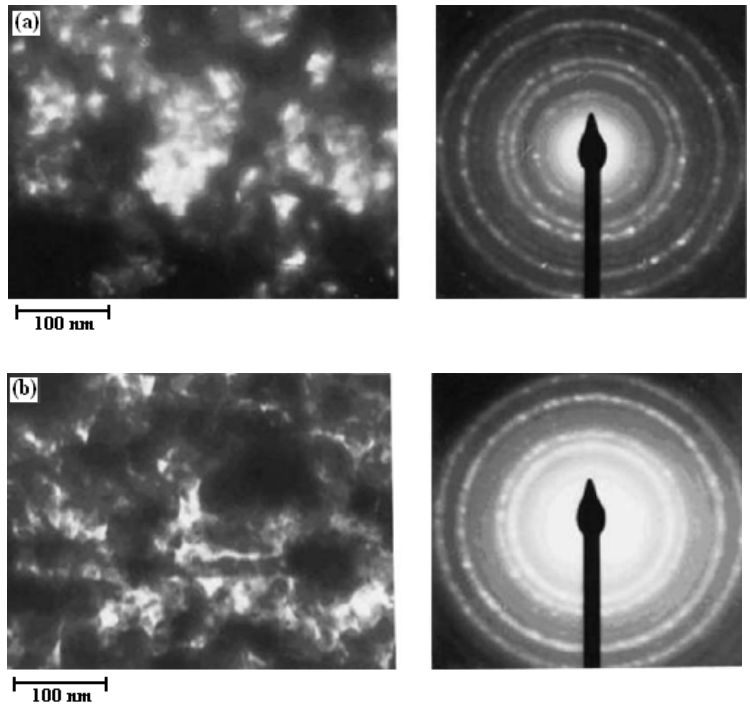

Fig. 4. TEM images and selected area diffraction patterns of $Ba_{0.5}Sr_{0.5}MoO_4$ nanopowders with 4 wt% CuO (a) and without CuO (b).

and 21.8 nm, respectively. As we can see, the results obtained from the TEM images correspond, with a slight difference, to those calculated using the Scherrer formula according to the XRD patterns. This slight difference between the XRD and TEM results seems to be within the acceptable range of errors possibly existing in our measurements.

Figure 4 also shows the diffraction pattern imaging of the produced powders with and without CuO. The sharp diffraction rings that appear in the diffraction pattern corresponds to the $Ba_{0.5}Sr_{0.5}MoO_4$ phase. As shown in Fig. 4, no amorphous phase can be detected in the diffraction pattern.

The improvement in the powder crystallinity improves the carrier mean free path in the lattice of the powder. Because of which, the generated carriers have less chances of scattering within the lattice. This contributes significantly to the improvement in the response of the sensor.

S is temperature-dependent and increases with temperature as the interaction at the gas-solid interface is accordingly enhanced. However, at a certain temperature, the thermal carrier generation mechanism overshadows the same caused by the interaction with the target gas. Also, the thermal desorption of the target gas molecules from the sensitive surface at higher temperatures becomes more significant and hinders the solid-gas interaction required for carrier generation.[29] Hence, it is important to find the maximum sensitivity temperature for the sample devices fabricated. In Fig. 5, the results of sensitivity measurements for the $Ba_{0.5}Sr_{0.5}MoO_4$ sensor without 4 wt% CuO at various operating temperatures are presented. In these experiments, the TGs were H_2S, H_2, LPG, and CO at 1000 ppm concentration. It is clear that the sensitivity to H_2S is more than to the other reducing gases. As expected, the sensitivity increases with increasing operating temperature (see Fig. 5). It can be seen from this figure that the sensitivity to H_2S increased and reached saturation values at approximately 250°C.

The major reason for the high sensitivity to H_2S relative to the other gases is as follows. A large amount of oxygen adsorped on the surface of the sensor at 250°C enables the sensor to oxidize H_2S immediately, giving a faster gas response.

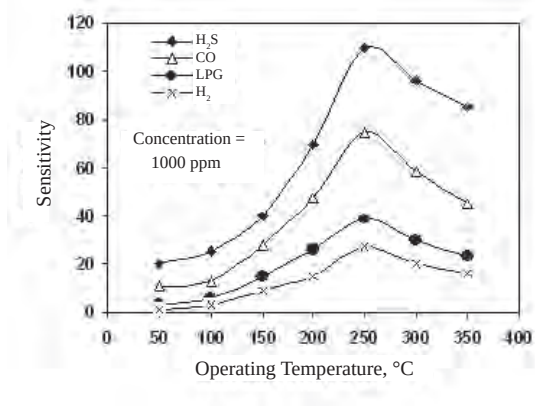

Fig. 5. Experimental relationship between sensitivity and operating temperature in gas sensors without CuO.

The sensitivities of sample devices to H_2S, H_2, LPG, and CO at 1000 ppm concentration with different weight percents of CuO at various operating temperatures were measured. The results are presented in Fig. 6, indicating the $Ba_{0.5}Sr_{0.5}MoO_4$ sensor with 4 wt% CuO was considerably outstanding in promoting the sensitivity than those with the other percentages of CuO. It was concluded that the maximum sensitivity of the fabricated sensors (Figs. 6(a)–6(d)) to the above-mentioned TGs occurred in the temperature range of 240–280°C. Accordingly, the rest of the measurements were carried out at a constant sensor temperature of 250°C. Also, it can be seen from Fig. 5 that the sensitivity of the sensing element with 4 wt% CuO to H_2S (Fig. 6(a)) is higher than those to other gases. Thus, the optimum amount of CuO as an additive is 4 wt% for the H_2S sensor element based on $Ba_{0.5}Sr_{0.5}MoO_4$.

The sensitivity as a function of the operating temperature for 4 wt% CuO: $Ba_{0.5}Sr_{0.5}MoO_4$ doped with different amounts (0.1 to 0.5 wt%) of Pd is shown in Fig. 7. It can be seen from Fig. 7 that the 4 wt% CuO: $Ba_{0.5}Sr_{0.5}MoO_4$ sensor doped with 0.3 wt% Pd has maximum sensitivity to H_2S at 200°C. With increasing the weight percent of Pd from 0.1 to 0.3 wt%, the sensitivity increases and it decreases above 0.3 wt%. This indicates that the dispersion of Pd has occurred on the surface of the semiconductor.

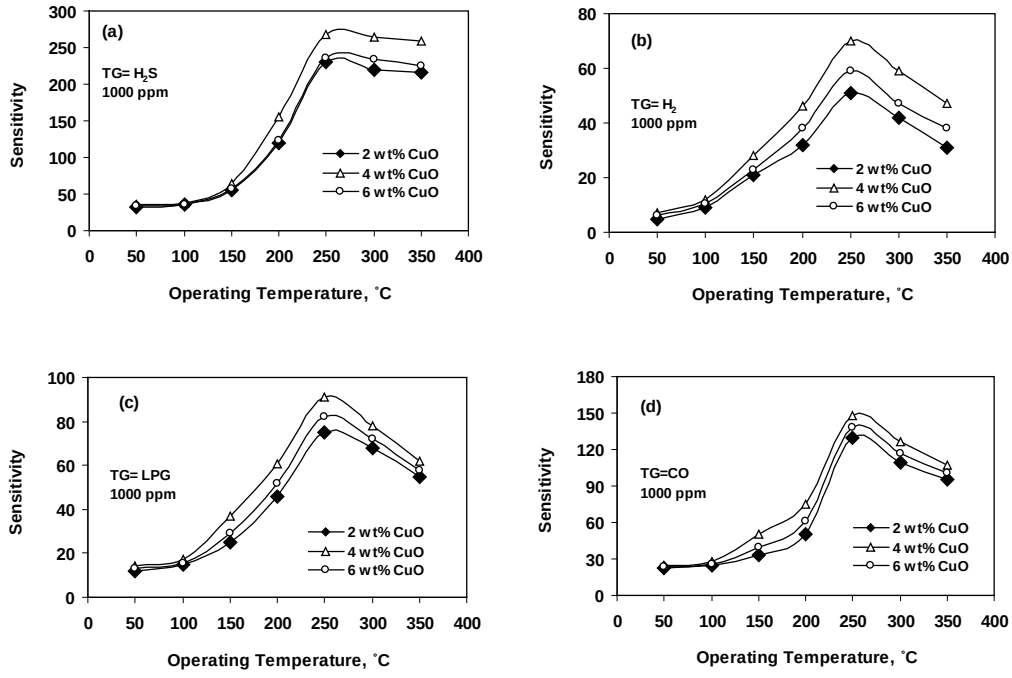

Fig. 6. Sensitivity of $Ba_{0.5}Sr_{0.5}MoO_4$ sensor with NiO at various weight percents (2, 4, and 6 wt %) vs operating temperature for sensing H_2S (a), H_2 (b), LPG (c), and CO (d).

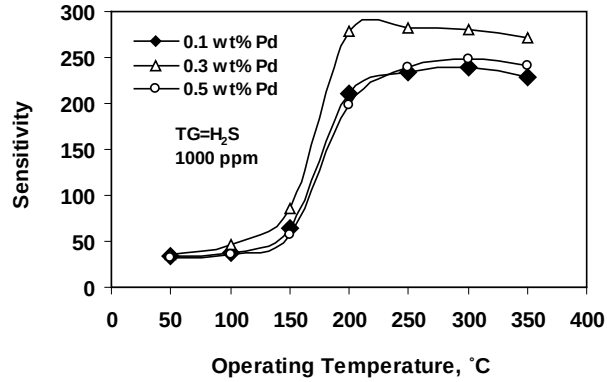

Fig. 7. Sensitivity vs operating temperature for 4 wt% CuO: $Ba_{0.5}Sr_{0.5}MoO_4$ sensor doped with different amounts of Pd.

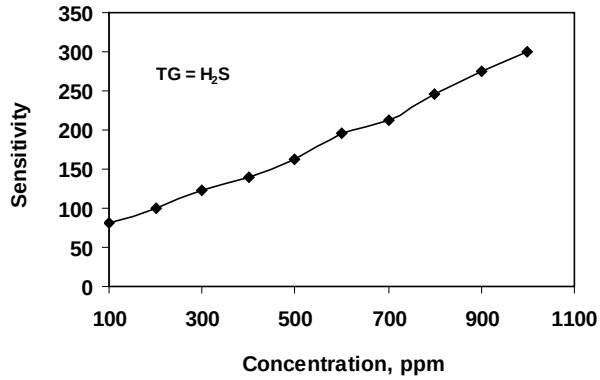

Fig. 8. Variations of sensitivity vs H_2S concentration in a fabricated sample gas sensor.

The sensitivities of a sample device (4 wt% CuO: $Ba_{0.5}Sr_{0.5}MoO_4$ doped with 0.3 wt% Pd) to various H_2S concentrations were measured. The results are presented in Fig. 8, indicating an almost linear increase in sensitivity with increasing TG concentration up to 1000 ppm. A saturation of sensitivity is observed for higher concentration levels.

4. Conclusion

Nanocrystalline $Ba_{0.5}Sr_{0.5}MoO_4$ thick films were deposited on an alumina tube using a simple and inexpensive sol-gel technique. These films were employed for the fabrication of $Ba_{0.5}Sr_{0.5}MoO_4$ gas sensors. Test devices were fabricated and their gas sensing characteristics with respect to H_2S, H_2, LPG, and CO gases were measured.

The elements based on $Ba_{0.5}Sr_{0.5}MoO_4$ incorporating 4 wt% CuO are highly sensitive to H_2S at an operating temperature of approximately 250°C. Doping of 4 wt% CuO: $Ba_{0.5}Sr_{0.5}MoO_4$ element with 0.3 wt% Pd decreases the operating temperature to 200°C and increases the sensitivity to H_2S.

References

1 N. Taguchi: US Patent, No. 3631436, 1971.
2 J. Watson and D. Tanner: Radio Electron Eng. **44** (1974) 85.
3 J. Tamaki, T. Maekawa, N. Miura and N. Yamazoe: Sens. Actuators, B **9** (1992) 197.
4 T. Oyabu: J. Appl. Phys. **53** (1982) 2785.
5 S. R. Morrison: Sens. Actuators, B **12** (1987) 425.
6 L. Bruno, C. Pijolat and R. Lalauze: Sens. Actuators, B **18–19** (1994) 195.
7 Y. Liu, W. Zhu, M. S. Tse and S. Y. Shen: J. Mater. Sci. Lett. **14** (1995), 1185.
8 H. Suo, F. Wu, Q. Wang, G. Liu, F. Qiu, B. Xu and M. Zhao: Sens. Actuators, B **45** (1997) 245.
9 T. Maekawa, J. Tamaki, N. Miura and N. Yamazoe: Chem. Lett. **20** (1991) 575.
10 A. Harkomamatilla, T. S. Rantala, V. Lantto and S. Leppavuori: Sens. Actuators, B **6** (1992) 248.
11 N. Yamazoe: Sens. Actuators, B **5** (1991) 7.
12 S. Shukla, L. Ludwig, C. Parrish and S. Seal: Sens. Actuators, B **104** (2005) 223.
13 S. Capone, M. Epifani, L. Francioso, S. Kaciulis, A. Mezzi, P. Siciliano and A. M. Taurino: Sens. Actuators, B **115** (2006) 396.
14 A. Hetznecker, H. Kohler and U. Guth: Sens. Actuators, B **120** (2007) 378.
15 B. Esfandyarpour, S. Mohajerzadeh, S. Famini, A. Khodadadi and E. Asl Soleimani: Sens. Actuators, B **100** (2004) 190.
16 L. Lisi, G. Bagnasco, P. Ciambelli, S. D. Rossi, A. P. Porta, A. G. Russo and M. Turco: J. Solid State Chem. **146** (1999) 176.
17 C. M. Chiu and Y. H. Chang: Thin Solid Films **342** (1999) 15.
18 Z. Y. Peng, X. Li, M. Y. Zhao, H. Cai, S. Q. Zhao and G. D. Hu: Thin Solid Films **286** (1999) 270.
19 C. M. Chiu and Y. H. Chang: Mater. Sci. Eng., A **266** (1999) 93.
20 C. M. Chiu and Y. H. Chang: Sens. Actuators, B **54** (1999), 236.
21 N. N. Toan, S. Saukko and V. Lantto: Physica B **327** (2003) 279.
22 F. Sher and J. P. Attfied: Solid States Sci. **8** (2006), 277.
23 M. Penza, C. Martucci and G. Cassano: Sens. Actuators, B **50** (1998) 52.
24 S. V. Manorama, C. V. Gopal and V. J. Rao: Appl. Surf. Sci. **174** (2001) 93.
25 M. S. Berberich, J. G. Zheng, U. Weimar, V. Gopel, N. Barsan, E. Pentia and A. Tomeaso: Sens. Actuators, B **31** (1996) 71.
26 H. F. Helegourc, F. Arefi, R. Planade and J. Amouroux: Sens. Actuators, B **73** (2001) 27.
27 T. Maekawa, K. Suzuki, T. Takada, T. Kobayashi and M. Egashira: Sens. Actuators, B **80** (2001) 51.
28 B. T. Marquis and J. F. Vetelino: Sens. Actuators, B **77** (2001) 100.
29 R. K. Sharma, P. C. H. Chan, Z. Tang, G. Yan, I. M. Hsing and J. K. O. Sin: Sens. Actuators, B **72** (2001) 160.